VIP Hollow Nanoparticles Very Important Paper

International Edition: DOI: 10.1002/anie.201706182
German Edition: DOI: 10.1002/ange.201706182

Unconventional Route to Uniform Hollow Semiconducting Nanoparticles with Tailorable Dimensions, Compositions, Surface Chemistry, and Near-Infrared Absorption

*Yanjie He, Xinchang Pang, Beibei Jiang, Chaowei Feng, Yeu-Wei Harn, Yihuang Chen, Young Jun Yoon, Shuang Pan, Cheng-Hsin Lu, Yajing Chang, Mona Zebarjadi, Zhitao Kang, Naresh Thadhani, Juan Peng, and Zhiqun Lin**

Abstract: *Despite impressive recent advances in the synthesis of lead chalcogenide solid nanoparticles, there are no examples of lead chalcogenide hollow nanoparticles (HNPs) with controlled diameter and shell thickness as current synthetic approaches for HNPs have inherent limitations associated with their complexity, inability to precisely control the dimensions, and limited possibilities with regard to applicable materials. Herein, we report on an unconventional strategy for crafting uniform lead chalcogenide (PbS and PbTe) HNPs with tailorable size, surface chemistry, and near-IR absorption. Amphiphilic star-like triblock copolymers [polystyrene-block-poly(acrylic acid)-block-polystyrene and polystyrene-block-poly(acrylic acid)-block-poly(3,4-ethylenedioxythiophene)] were rationally synthesized and exploited as nanoreactors for the formation of uniform PbS and PbTe HNPs. Compared to their solid counterparts, the near-IR absorption of the HNPs is blue-shifted owing to the hollow interior. This strategy can be readily extended to other types of intriguing low-band-gap HNPs for diverse applications.*

The ability to control the size, shape, and structure of colloidal nanoparticles (NPs) is of fundamental and technological importance as the optical, electrical, optoelectronic, magnetic, and catalytic properties of NPs depend heavily on these parameters.[1–3] Whereas solid NPs have a positive curvature, hollow NPs (HNPs) also possess a negative curvature on the inner surface,[4] and represent an important class of nanomaterials. They have received considerable attention owing to their much higher surface area to volume ratio compared to solid counterparts of the same size for potential applications, for example, in drug delivery, bioimaging, and photothermal therapy.[5]

The synthetic routes to HNPs can be broadly grouped into four categories based on the formation mechanism of the hollow structures: nanoscale Kirkendall effect,[6,7] galvanic replacement reactions,[8,9] preferential chemical etching,[10] and template-mediated approaches.[11] In spite of their effectiveness in synthesizing a variety of HNPs with good morphological control, the materials that are amenable to each approach are inherently limited in scope. For instance, the use of the nanoscale Kirkendall effect has been recognized as a robust strategy towards HNPs.[6] However, precisely tuning the diameter of the hollow interior and the shell thickness as well as the composition of the HNPs remains challenging, particularly considering that various parameters such as the temperature, diffusion rate, and concentration profiles of atoms, and the specific geometry of HNPs are usually correlated with each other and complicate the diffusion process of the Kirkendall effect.[12] Consequently, this approach is greatly restricted to the synthesis of metal oxide, transition-metal sulfide, and selenide HNPs.[13,14] The second viable approach for the synthesis of HNPs is galvanic replacement,[8] which is highly effective in the self-templating production of noble-metal HNPs with well-controlled hollow nanostructures. Although this approach has also been extended to the synthesis of metal oxide HNPs,[15] it is primarily employed to prepare noble-metal HNPs.[9,16] Preferential chemical etching is the third feasible approach to obtain HNPs with well-defined hollow interiors. However, this method is mainly utilized to synthesize metal oxide HNPs, and often requires high temperatures to promote the etching process.[5] Lastly, (hard or soft) template-mediated approaches enable the preparation of a diverse range of HNPs but still suffer from several limitations. For hard template approaches, the availability and size of a suitable template (usually larger than 50 nm) as well as the homogeneous nucleation during the coating process make it difficult to control the morphology of the HNPs in a reproducible manner, and template removal after the treatment is also a major issue (e.g., removal of silica templates invokes the use of hydrofluoric acid).[11] On the

[*] Y. He, Dr. X. Pang, Dr. B. Jiang, Dr. C. Feng, Y.-W. Harn, Dr. Y. Chen, Y. J. Yoon, S. Pan, Dr. C.-H. Lu, Y. Chang, Prof. N. Thadhani, Prof. Z. Lin
School of Materials Science and Engineering
Georgia Institute of Technology
Atlanta, GA 30332 (USA)
E-mail: zhiqun.lin@mse.gatech.edu
Homepage: http://nanofm.mse.gatech.edu/

Dr. Z. Kang
Electronic System Laboratory
Georgia Tech Research Institute
Atlanta, GA 30332 (USA)

Prof. M. Zebarjadi
Department of Electrical and Computer Engineering
University of Virginia
Charlottesville, VA 22904 (USA)

Prof. J. Peng
Department of Macromolecular Science
Fudan University, Shanghai, 200433 (China)

Supporting information and the ORCID identification number(s) for the author(s) of this article can be found under: https://doi.org/10.1002/anie.201706182.

other hand, it is still challenging to implement soft templates (e.g., micelles formed by self-assembly of linear block copolymers) for the synthesis of HNPs as these self-assembled templates may be destabilized upon variations in the experimental conditions, such as the pH, temperature, or solvent.[17]

Recent research has witnessed rapid advances in the synthesis of a myriad of high-quality colloidal nanocrystals.[2,3,6] Among the IV–VI semiconductor nanocrystals, low-band-gap lead chalcogenide NPs are of particular interest as they possess much broader size-tunable optoelectronic properties from the visible to the near-IR region that open up opportunities for their use in solar energy conversion,[18] thermoelectric devices,[19] and photodetectors.[20] It is noteworthy that the synthesis of lead chalcogenide solid NPs, for example, PbTe, often requires the use of trialkylphosphine ligands (e.g., trioctylphosphine (TOP), trioctylphosphine oxide (TOPO), and tributyl phosphate (TBP)) because of the poor solubility of tellurium in most organic solvents.[21–26] To the best of our knowledge, no synthetic strategies have been reported for crafting uniform lead chalcogenide HNPs with negatively curved hollow structures, which is largely due to the limitations associated with the conventional approaches described above. Moreover, lead chalcogenide NPs are susceptible to degradation upon exposure to air and water; this further aggravates the daunting challenge in synthesizing lead chalcogenide HNPs with tunable surface properties. It is important to note that theoretical modeling suggests that the presence of the hollow interior in semiconducting nanostructures offers another unique ability to tailor their size- and structure-dependent properties.[27,28]

Herein, we report on an unconventional yet robust strategy for the synthesis of uniform low-band-gap semiconducting HNPs with tailorable size, surface chemistry, and near-IR absorption that capitalizes on judiciously designed amphiphilic star-like triblock copolymers as nanoreactors. These nanoreactors were based on polystyrene-*block*-poly(acrylic acid)-*block*-polystyrene (PS-*b*-PAA-*b*-PS) and polystyrene-*block*-poly(acrylic acid)-*block*-poly(3,4-ethylenedioxythiophene) (PS-*b*-PAA-*b*-PEDOT). The former one was synthesized by three consecutive atom transfer radical polymerization (ATRP) reactions, and the latter one was prepared by two sequential ATRP reactions in conjunction with a click reaction and a Grignard metathesis polymerization. Two lead chalcogenide HNPs (PbTe and PbS) with easily controllable shell thicknesses were crafted to demonstrate the effectiveness of this strategy. In sharp contrast to the conventional approaches towards HNPs described above, the synthetic strategy developed in this study not only offers an alkylphosphine-free approach towards PbTe and PbS HNPs (i.e., with reactions in the absence of TOP, TBP, and TOPO), but also enables the in situ crafting of HNPs with tunable surface chemistry (the surface capping ligand can be readily changed from hydrophobic PS to conjugated PEDOT). More importantly, compared to solid counterparts of the same size, the as-synthesized HNPs exhibited a blue-shift in absorption owing to the hollow interior, which experimentally confirmed the change in the optical band gap of semiconducting HNPs predicted by a theoretical model based on the bond order–length–strength correlation mechanism using a local bond average approach.[28] These low-band-gap HNPs can be exploited either as building blocks for the construction of assemblies or as materials for energy conversion and storage or sensors, for example.

The synthetic routes towards uniform PbS and PbTe HNPs capped with coil-like PS and rod-like conjugated PEDOT as ligands on the surface capitalized on amphiphilic star-like PS-*b*-PAA-*b*-PS and PS-*b*-PAA-*b*-PEDOT triblock copolymers, respectively, as nanoreactors (Figure 1). The amphiphilic star-like PS-*b*-PAA-*b*-PS triblock copolymers were synthesized by sequential ATRP of styrene (St), *tert*-butyl acrylate (*t*BA), and St to form PS-*b*-P*t*BA-*b*-PS (Figure 1, second row) using brominated β-cyclodextrin (21Br-β-CD) as the macroinitiator (top row), followed by hydrolysis of the intermediate P*t*BA blocks into PAA. The 21 hydroxy groups on β-CD were transformed into ATRP initiation sites through an esterification reaction between β-CD and α-bromoisobutyryl bromide with nearly 100% conversion, as confirmed by ^{1}H NMR spectroscopy (see the Supporting Information, Figure S1), and 21-arm, star-like PS-*b*-P*t*BA-*b*-PS was thus afforded (Figure S2). All of the as-prepared star-like polymers exhibited monomodal gel permeation chromatography (GPC) traces (Figure S3) and narrow M_w distributions (polydispersity index, PDI < 1.16).

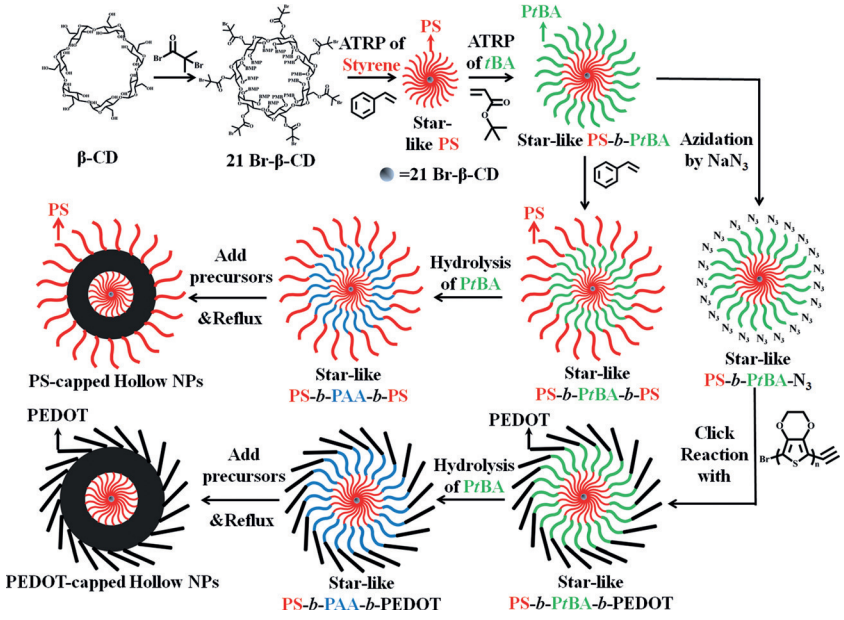

Figure 1. Stepwise representation of the synthesis of low-band-gap HNPs with tunable dimensions and surface chemistry with star-like PS-*b*-PAA-*b*-PS or PS-*b*-PAA-*b*-PEDOT triblock copolymers as nanoreactors.

Notably, symmetric peaks were observed in all GPC measurements, suggesting that there is no intermolecular coupling during the ATRP reaction. To obtain uniform HNPs, it is critical to remove linear homopolymer P*t*BA (formed by the second ATRP) side products from the star-like PS-*b*-P*t*BA diblock copolymers by fractional precipitation using acetone as the solvent and methanol/water as the precipitator (Figure S3b,c). The presence of linear P*t*BA homopolymer would interfere with the NP formation, producing a large amount of irregular structures. The *tert*-butyl substituents in the intermediate P*t*BA block of star-like PS-*b*-P*t*BA-*b*-PS can be easily hydrolyzed, thereby yielding amphiphilic star-like PS-*b*-PAA-*b*-PS. The successful synthesis of unimolecular star-like PS-*b*-PAA-*b*-PS nanoreactors was confirmed by DLS measurements, which indicated their uniform size in dimethylformamide (DMF; Figure S4).

The resulting star-like PS-*b*-PAA-*b*-PS triblock copolymers were then utilized as nanoreactors for the synthesis of uniform PbTe and PbS HNPs. The reactions were performed in a mixed solvent composed of DMF/benzyl alcohol (DMF/BA). Low-band-gap PbTe HNPs were first produced to demonstrate the effectiveness of capitalizing on star-like PS-*b*-PAA-*b*-PS as nanoreactors to yield uniform HNPs. The star-like PS-*b*-PAA-*b*-PS triblock copolymers were first dissolved in DMF/BA to form stable unimolecular spherical nanoreactors. Separately prepared[29] PbTe precursors were added into the star-like PS-*b*-PAA-*b*-PS DMF/BA solution, followed by reflux at 160 °C. DMF is a good solvent for both PS and PAA blocks whereas BA is a good solvent for PAA and a poor solvent for PS. As a result, stable unimolecular micelles with well-defined spherical shapes with expanded intermediate PAA chains and collapsed inner and outer PS chains were formed in the mixed DMF/BA. The precursors were selectively partitioned into the hydrophilic PAA regime, which can accommodate a large volume of precursors owing to the expanded PAA chain conformation, and the strong coordinating interaction between the carboxylic acid groups of PAA and the metal atoms of the PbTe precursors in the compartment formed by the PAA blocks led to the nucleation and growth of PbTe HNPs tethered with PS chains inside the hollow interior and on the outside of the HNPs. As the outer PS blocks are originally covalently connected to the intermediate PAA blocks, the surface of a PbTe HNP is intimately and permanently capped with PS blocks, which leads to good solubility in various common organic solvents (polar and nonpolar solvents).

A representative transmission electron microscopy (TEM) image of the PbTe HNPs with an average hollow interior diameter $D_{hollow} = 3.5 \pm 0.2$ nm and a shell thickness $t_{shell} = 2.8 \pm 0.2$ nm crafted by exploiting star-like PS-*b*-PAA-*b*-PS nanoreactors (sample A in Table S1) is shown in Figure 2a. The existence of the hollow interior in the PS-capped PbTe HNPs is clearly evident from the brightness of the center of each individual HNP (HRTEM imaging; Figure 2a, inset). The lattice spacing is consistent with the (220) interplanar distance of 0.23 nm of face-centered cubic PbTe. The formation of the hollow interior can be ascribed to the fact that the inner PS blocks do not possess functional groups for coordination with the metal moieties of the PbTe precursors and thus only serve as a nanoscopic scaffold. As noted above, owing to the controlled living nature of the ATRP, the molecular weights of the inner PS and the intermediate PAA blocks and thus the diameter of the hollow interior and the thickness of the PbTe shell of the PbTe HNPs can be readily tuned by varying the ATRP time of the inner PS and intermediate P*t*BA (later hydrolyzed into PAA) blocks, respectively. PbTe HNPs with different dimensions ($D_{hollow} = 1.8 \pm 0.2$ nm and $t_{shell} = 4.6 \pm 0.4$ nm), which were prepared by using different star-like triblock copolymers as nanoreactors (sample B in Table S1), are shown in Figure 2b. Note that the lattice spacing is again consistent with the (200) interplanar distance of 0.32 nm.

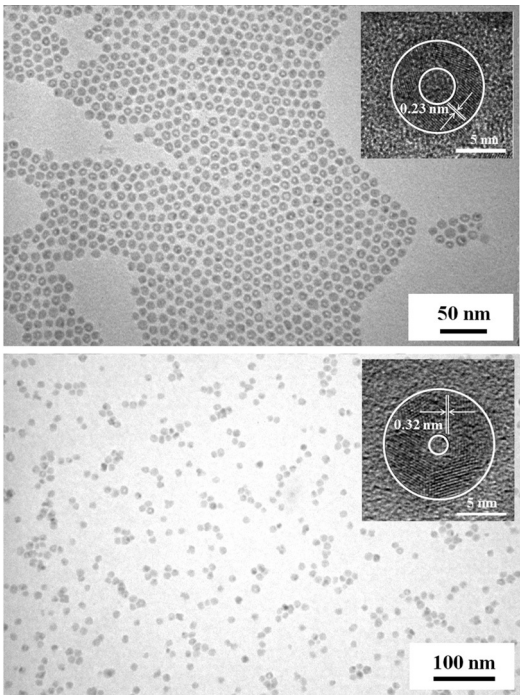

Figure 2. TEM images of PS-capped PbTe HNPs with a) a hollow interior diameter of $D_{hollow} = 3.5 \pm 0.2$ nm and a shell thickness of $t_{shell} = 2.8 \pm 0.2$ nm (inset: HRTEM of PbTe HNPs), and b) $D_{hollow} = 1.8 \pm 0.2$ nm and $t_{shell} = 4.6 \pm 0.4$ nm (inset: HRTEM of PbTe HNPs), crafted by capitalizing on star-like PS-*b*-PAA-*b*-PS polymers as nanoreactors. The white circles in the insets are for guidance only and indicate the shell thickness of the HNPs.

To further substantiate that the formation of HNPs was structure-directed by the intermediate hydrophilic PAA blocks, two control experiments were conducted with star-like PS-*b*-P*t*BA-*b*-PS and linear PS-*b*-PAA-*b*-PS triblock copolymers as nanoreactors to grow HNPs. Obviously, compared to the carboxylic acid groups of PAA, the *tert*-butyl groups in the P*t*BA sections of the star-like PS-*b*-P*t*BA-*b*-PS triblock copolymers cannot selectively sequester precursors dissolved in DMF/BA owing to the lack of ability to coordinate with the metal moieties in the PbTe precursors. Consequently, PbTe structures with irregular morphologies were obtained (Figure S5a). On the other hand, the use of linear PS-*b*-PAA-*b*-PS block copolymers also failed to produce HNPs as the linear copolymers were not able to form thermodynamically stable micelles at 160 °C (because of

dissociation of the micelles at high temperature). Only aggregates were thus observed (Figure S5b).

It is notable that conventional synthetic approaches to metal chalcogenide NPs require temporally discrete homogenous nucleation induced by hot injection of reagents, followed by steady crystallite growth upon re-heating, thereby leading to the formation of metal chalcogenide NPs.[22] According to classical nucleation theory, there is a critical radius above which the growth of nuclei is energetically favorable. Clearly, the growth of HNPs invokes a higher thermodynamic energy barrier that is due to the creation of an interior surface. Thus nuclei with hollow interiors tend to spontaneously dissolve back to solution. In other words, the formation of nuclei with hollow interiors is thermodynamically unfavorable. As a result, conventional approaches (e.g., Kirkendall effect, galvanic replacement, chemical etching) usually involve the synthesis of sacrificial solid nanocrystals with positive curvature, followed by post-synthesis procedures (e.g., oxidation, etching) to transform the solid core into a hollow interior (to create a negative curvature inside the HNPs). The energy barrier that is due to the creation of the hollow interior can thus be mediated by this two-step process, enabling the thermodynamically favorable conversion of solid NPs into HNPs.

In stark contrast to the approaches described above, our nanoreactor strategy can circumvent the classical nucleation issue associated with the formation of HNPs by utilizing amphiphilic star-like PS-*b*-PAA-*b*-PS triblock copolymers as nanoreactors to template the growth of PbTe confined in the compartment populated by the intermediate PAA blocks and to eventually form PbTe HNPs in a one-step process, obviating the need for any sacrificial templates. It is important to note that the dispersion of PbTe HNPs can be stabilized by the presence of the PS chains tethered onto the surface of the HNPs. This was substantiated by the observation of flocculation in a PbTe HNP toluene solution when a non-solvent (ethanol) for PS was introduced into the solution (Figure S6e). In addition, as most trialkylphosphine compounds are non-polar, the solid PbTe NPs prepared by conventional approaches display very poor solubility in polar organic solvents,[22] such as DMF, dimethyl sulfoxide (DMSO), and dimethylacetamide (DMA). It is not surprising that because of the excellent solubility of PS in a wide range of organic solvents, as-synthesized PS-capped PbTe HNPs possess superior solubility and stability not only in non-polar solvents (e.g., chlorobenzene, toluene; Figure S6a,b), but also in polar solvents (e.g., DMF, DMA; Figure S6c,d).

Figure S7a depicts the X-ray diffraction (XRD) profile and SAED pattern of PS-capped PbTe HNPs synthesized with star-like PS-*b*-PAA-*b*-PS as the nanoreactor (sample A in Table S1). The diffraction peaks can be indexed to the face-centered cubic phase of PbTe, and are consistent with the standard XRD profile of bulk PbTe. The broadening of the diffraction peaks can be ascribed to the small crystalline size of the resulting PbTe HNPs. The corresponding energy dispersive X-ray (EDX) analysis (Figure S7b) further confirmed that the atomic ratio of Pb to Te was 1:1.

Notably, by judiciously designing the outer polymer blocks, a variety of functional polymers (e.g., conjugated polymers) can be placed on the surface of the HNPs as ligands, which leads to great surface chemistry tunability. To the best of our knowledge, there are currently no strategies for the one-step synthesis of HNPs tethered to semiconducting ligands. Compared to classical routes towards molecular metal chalcogenide complexes, which are based on the use of highly toxic and explosive hydrazine,[30] our approach offers a hydrazine-free method that maintains both the complete functionality of the semiconducting ligands and the colloidal stability of the low-band-gap HNPs.

In this context, we crafted conjugated-polymer-capped PbTe HNPs by employing the star-like PS-*b*-PAA-*b*-PEDOT triblock copolymers as nanoreactors. Specifically, star-like PS-*b*-P*t*BA-N_3 was synthesized by sequential ATRP of St and *t*BA, followed by post-polymerization S_N2 reactions of the terminal bromine groups with NaN_3. The success of the azidation reactions was confirmed by the appearance of a band at 2100 cm^{-1} in the FTIR spectrum, which is characteristic for the stretching of an -N_3 group (Figure S8a). The success of the click reaction was confirmed by the emergence of the absorption peaks of PEDOT in the visible

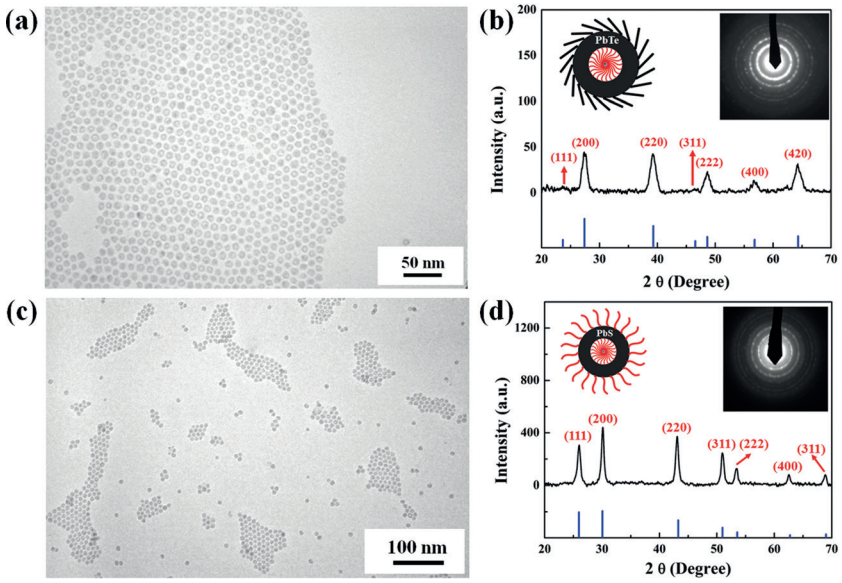

Figure 3. a) TEM image and b) XRD profile of PbTe HNPs capped with conjugated PEDOT with $t_{shell} = 3.1 \pm 0.3$ nm and $D_{hollow} = 3.2 \pm 0.3$ nm crafted by employing star-like PS-*b*-PAA-*b*-PEDOT as nanoreactors. The blue lines represent the standard XRD pattern of bulk PbTe. Inset: SAED pattern of PEDOT-capped PbTe HNPs. c) TEM image and d) XRD profile of PS-capped PbS HNPs with $t_{shell} = 2.9 \pm 0.2$ nm and $D_{hollow} = 3.6 \pm 0.2$ nm crafted by utilizing star-like PS-*b*-PAA-*b*-PS as nanoreactors. The blue lines represent the standard XRD pattern of bulk PbS. Inset: SAED pattern of PS-capped PbS HNPs.

region (Figure S9).[31] Similar to the synthesis of PS-capped PbTe HNPs, the PbTe HNPs with PEDOT caps were crafted using sample C in Table S1 as the nanoreactor. A TEM image, XRD profile, and SAED pattern of the PEDOT-capped PbTe HNPs ($D_{hollow} = 3.2 \pm 0.3$ nm and $t_{shell} = 3.1 \pm 0.3$ nm) are shown in Figure 3a and b. Clearly, the change in the surface ligands from insulating PS to conjugated PEDOT did not affect the HNP morphology, signifying that our star-like block copolymer strategy imparts good surface ligand tunability while maintaining HNP morphology. EDX analysis confirmed the 1:1 ratio of Pb and Te (Figure S10a). The ability to stably tether conjugated polymers onto low-band-gap NPs provides opportunities for their use in thermoelectric devices and solar cells and obviates the need for ligand exchange of insulating ligands with conjugated polymers as in copious past studies. Notably, as the surface chemistry was rendered tunable by a click reaction between conjugated PEDOT and star-like PS-*b*-P*t*BA diblock copolymers (Figure 1), we envision that a diverse range of other conjugated polymers (e.g., poly(3-hexylthiophene)) can be readily grafted to eventually yield PbTe HNPs capped with different conjugated polymers of interest for potential applications in optoelectronic devices.

Aside from its possibilities for HNP surface tuning, our nanoreactor strategy is robust and enables the crafting of other lead chalcogenide HNPs (i.e., PbS). PbS HNPs were produced by using star-like PS-*b*-PAA-*b*-PS copolymers as the nanoreactors (Figure 3c; $D_{hollow} = 2.9 \pm 0.2$ nm and $t_{shell} = 3.6 \pm 0.2$ nm). The structure and chemical composition of the resulting PS-capped PbS HNPs were confirmed by XRD (Figure 3d) and EDX (Figure S10b) analysis, respectively, and their growth mechanism is similar to that of the PS-capped PbTe HNPs.

Interestingly, the presence of negative curvature exerted an influence on the absorption spectrum of the HNPs. It is well-known that a reduction in the NP size increases the fraction of surface atoms, which have lower coordination numbers (CNs) than the atoms located in the core of NPs. The most pronounced distinction between HNPs and solid NPs is the increase in the fraction of uncoordinated atoms owing to the presence of the hollow interior, leading to a decrease in the average CN of an individual HNP. The optical band gap, which originates from the crystal potential, is dependent upon the first Fourier coefficient of the crystal field, which is proportional to the average cohesive energy per bond.[32] The decrease in the mean CN of an individual HNP as a result of the hollow interior causes an increase in the average cohesive energy per bond, which in turn leads to an increase in the optical band gap of the resulting lead chalcogenide HNPs. The blue-shift of the absorption band (Figure 4) can be semi-quantitatively rationalized by Equation (1).[32,33]

$$\Delta E_g(R,r) = E_g(B)\left\{\frac{z_b}{\langle z\rangle}\left[\tau_{in}\left(\sqrt{z_{in,B}}-1\right)+\tau_{out}\left(\sqrt{z_{out,B}}-1\right)+1\right] - \frac{z_b}{\langle z\rangle}\left[\tau\left(\sqrt{z_{s,B}}-1\right)+1\right]\right\} \quad (1)$$

A detailed explanation of each individual parameter can be found in the Supporting Information. Based on this equation, it is predicted that $\Delta E_g(R,r) > 0$,[32,33] suggesting an increased optical band gap for HNPs, and thus a blue-shift in the absorption maximum for HNPs compared to their solid counterparts. The PbS HNPs prepared with copolymer nanoreactors experimentally confirmed this prediction for lead chalcogenide HNPs.

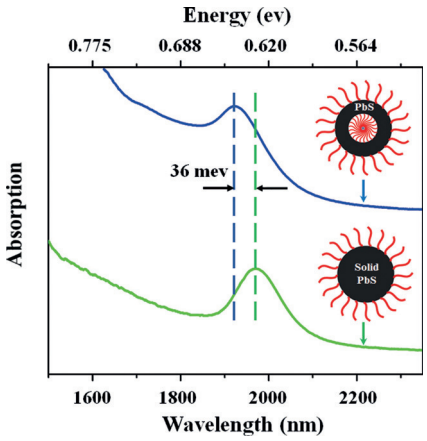

Figure 4. Near-infrared (NIR) spectra of PS-capped PbS HNPs with $t_{shell} = 2.9 \pm 0.2$ nm and $D_{hollow} = 3.6 \pm 0.2$ nm crafted by utilizing star-like PS-*b*-PAA-*b*-PS as nanoreactors and of PS-capped PbS solid NPs with the same external diameter prepared by utilizing star-like PAA-*b*-PS as nanoreactors.

In summary, we have developed a viable strategy based on the use of star-like triblock copolymer nanoreactors for the synthesis of uniform low-band-gap lead chalcogenide HNPs with readily and independently tailorable dimensions (diameter of the hollow interior and shell thickness), compositions (PbTe and PbS), and surface chemistry (capping with hydrophobic PS or conjugated PEDOT), which are not easily accessible by conventional approaches. The growth of lead chalcogenides is facilitated by the strong coordination between the PAA blocks and the metal atoms of the precursors. Importantly, compared to solid NPs with the same external diameter, lead chalcogenide HNPs exhibited an absorption maximum blue-shift that is due to the hollow interior, which is in good agreement with theoretical predictions. Clearly, the star-like triblock copolymer nanoreactor strategy may enable the synthesis of an exciting, virtually unlimited variety of uniform polymer-capped HNPs of different sizes, materials, and surface functional ligands. As such, it represents a general and robust strategy for producing functional low-band-gap HNPs and exploring how internal (e.g., dimension, composition, and surface ligand) and external (e.g., light, pH, temperature, and magnetic and electric fields) parameters influence the physical properties of HNPs and their assemblies for a wide range of applications in solar energy conversion (e.g., quantum dot solar cells, light-emitting diodes, and near-IR photodetectors), thermoelectric devices, batteries, sensors, and bioimaging.

Acknowledgements

We gratefully acknowledge funding support from the Air Force Office of Scientific Research (FA9550-16-1-0187), the

National Science Foundation (CMMI 1562075), and the National Natural Science Foundation of China (21674024). Support by Independent Research and Development funding from Georgia Tech Research Institute is also acknowledged.

Conflict of interest

The authors declare no conflict of interest.

Keywords: block copolymers · hollow nanoparticles · lead chalcogenides · nanoreactors · near-infrared absorption

How to cite: *Angew. Chem. Int. Ed.* **2017**, *56*, 12946–12951
Angew. Chem. **2017**, *129*, 13126–13131

[1] L. H. Qu, Z. A. Peng, X. G. Peng, *Nano. Lett.* **2001**, *1*, 333.
[2] D. J. Milliron, S. M. Hughes, Y. Cui, L. Manna, J. Li, L. Wang, A. P. Alivisatos, *Nature* **2004**, *430*, 190.
[3] J. Ge, Y. Xu, Y. Yin, *Angew. Chem. Int. Ed.* **2007**, *46*, 7428; *Angew. Chem.* **2007**, *119*, 7572.
[4] L. I. Hung, C. K. Tsung, W. Y. Huang, P. D. Yang, *Adv. Mater.* **2010**, *22*, 1910.
[5] K. An, T. Hyeon, *Nano Today* **2009**, *4*, 359.
[6] Y. Yin, R. M. Rioux, C. K. Erdonmez, S. Hughes, G. A. Somorjal, A. P. Alivisatos, *Science* **2004**, *304*, 711.
[7] S. Peng, S. H. Sun, *Angew. Chem. Int. Ed.* **2007**, *46*, 4155; *Angew. Chem.* **2007**, *119*, 4233.
[8] Y. G. Sun, B. T. Mayers, Y. N. Xia, *Nano. Lett.* **2002**, *2*, 481.
[9] Y. G. Sun, Y. N. Xia, *J. Am. Chem. Soc.* **2004**, *126*, 3892.
[10] D. Kim, J. Park, K. An, N. K. Yang, J. G. Park, T. Hyeon, *J. Am. Chem. Soc.* **2007**, *129*, 5812.
[11] Q. Zhang, W. S. Wang, J. Goebl, Y. D. Yin, *Nano Today* **2009**, *4*, 494.
[12] H. J. Fan, U. Gosele, M. Zacharias, *Small* **2007**, *3*, 1660.
[13] J. G. Railsback, A. C. Johnston-Peck, J. W. Wang, J. B. Tracy, *ACS Nano* **2010**, *4*, 1913.
[14] A. Cabot, M. Ibanez, P. Guardia, A. P. Alivisatos, *J. Am. Chem. Soc.* **2009**, *131*, 11326.
[15] M. H. Oh, T. Yu, S. H. Yu, B. Lim, K. T. Ko, M. Willinger, D. H. Seo, B. H. Kim, M. G. Cho, J. H. Park, K. Kang, Y. E. Sung, N. Pinna, T. Hyeon, *Science* **2013**, *340*, 964.
[16] X. H. Xia, Y. Wang, A. Ruditskiy, Y. N. Xia, *Adv. Mater.* **2013**, *25*, 6313.
[17] X. C. Pang, L. Zhao, W. Han, X. K. Xin, Z. Q. Lin, *Nat. Nanotechnol.* **2013**, *8*, 426.
[18] M. L. Böhm, T. C. Jellicoe, M. Tabachnyk, N. J. Davis, F. Wisnivesky-Rocca-Rivarola, C. Ducati, B. Ehrier, A. Bakulin, N. C. Greenham, *Nano Lett.* **2015**, *15*, 7987.
[19] S. W. Finefrock, Y. Wang, J. B. Ferguson, V. J. Ward, H. Fang, J. E. Pfluger, D. S. Dudis, X. Ruan, Y. Wu, *Nano Lett.* **2013**, *13*, 5006.
[20] R. Saran, R. J. Curry, *Nat. Photonics* **2016**, *10*, 81.
[21] C. B. Murray, D. J. Norris, M. G. Bawendi, *J. Am. Chem. Soc.* **1993**, *115*, 8706.
[22] J. J. Urban, D. V. Talapin, E. V. Shevchenko, C. B. Murray, *J. Am. Chem. Soc.* **2006**, *128*, 3248.
[23] W. G. Lu, J. Y. Fang, K. L. Stokes, J. Lin, *J. Am. Chem. Soc.* **2004**, *126*, 11798.
[24] J. E. Murphy, M. C. Beard, A. G. Norman, S. P. Ahrenkiel, J. C. Johnson, P. Yu, O. I. Micic, R. J. Ellingson, A. J. Nozik, *J. Am. Chem. Soc.* **2006**, *128*, 3241.
[25] H. Shen, H. Wang, X. Chen, J. Z. Niu, W. Xu, X. M. Li, X. Jiang, Z. Du, L. Song, *Chem. Mater.* **2010**, *22*, 4756.
[26] T. L. Mokari, M. J. Zhang, P. D. Yang, *J. Am. Chem. Soc.* **2007**, *129*, 9864.
[27] H. Zeng, W. Cai, P. Liu, X. Xu, H. Zhou, C. Klingshirn, H. Kalt, *ACS Nano* **2008**, *2*, 1661.
[28] C. Q. Sun, *Prog. Solid State Chem.* **2007**, *35*, 1.
[29] N. Ziqubu, K. Ramasamy, P. V. S. R. Rajasekhar, N. Revaprasadu, P. OBrien, *Chem. Mater.* **2010**, *22*, 3817.
[30] M. V. Kovalenko, M. Scheele, D. V. Talapin, *Science* **2009**, *324*, 1417.
[31] F. Tran-Van, S. Garreau, G. Louarn, G. Froyer, C. Chevrot, *J. Mater. Chem.* **2001**, *11*, 1378.
[32] G. Ouyang, G. W. Yang, *IEEE Trans. Nanotechnol.* **2012**, *11*, 866.
[33] G. Ouyang, G. W. Yang, *ACS Appl. Mater. Interfaces* **2012**, *4*, 210.

Manuscript received: June 17, 2017
Accepted manuscript online: July 18, 2017
Version of record online: August 10, 2017

